

Qudit vs. Qubit: Simulated performance of error correction codes in higher dimensions

James Keppens^{1,2,*}, Quinten Eggerickx^{1,2,3}, Vukan Levajac^{1,4}, George Simion¹, and Bart Sorée¹

¹*Imec, Leuven, Belgium*

²*Department of Electrical Engineering, KU Leuven, Leuven, Belgium*

³*Department of Physics, UGent, Ghent, Belgium and*

⁴*Department of Physics, KU Leuven, Leuven, Belgium*

(Dated: February 11, 2025)

Qudits can be described by a state vector in a q -dimensional Hilbert space, enabling a more extensive encoding and manipulation of information compared to qubits. This implies that conducting fault tolerant quantum computations using qudits rather than qubits might entail less overhead. We test this hypothesis by creating and simulating the quantum circuitry for small qudit error correction codes and specifically adapted decoders and compare the simulated performance with their qubit counterparts under two different noise models. We introduce an error ratio to quantify the trade-off between logical error rates and the reduction in the number of units required when using qudits. We find that the logical error rates of our simulated distance-3 codes would give less average computational errors for the higher dimensional codes, especially when the decoder can be adapted to correct more hyperedge-type errors.

1. INTRODUCTION

One of the main obstacles in advancing practical quantum computing lies in the significant susceptibility of quantum systems to noise [1]. At present, the most promising approach to address this issue is through the utilization of error correction codes, an approach recently proven to work effectively in experiments conducted by Google Quantum AI and collaborators [2]. These codes combine n physical qubits to construct k logical units of which the logical states are separated by a distance d . Today's most practical code, the surface code [3, 4], suffers from a sub-optimal scaling between n and d . Additionally, it lacks an efficient method to perform certain logical gates, necessitating an excessive number of qubits to achieve satisfactory logical error levels for the execution of quantum algorithms. Efforts to address these problems involve research into linear high-distance Low-Density-Parity-Check (LDPC) codes [5, 6], and Non-Abelian codes [7, 8]. While these methods show promise, the majority of proposed codes either remain confined to acting solely as quantum memories or still entail excessive overhead requirements. Another approach to mitigate the overhead associated with quantum error correction codes involves the utilization of multilevel systems.

Qudits are q -level quantum mechanical systems, capable of storing and processing the same amount of information as $\log_2(q)$ qubits. Moreover, their extended complete gate set governed by $\otimes SU(q)$ allows for some more fundamental theoretical advantages [9–11]. Leveraging qudits for fault-tolerant schemes can thus offer improved scaling options and enhanced methods to perform logical gates [12, 13], provided that the fabrication and control of qudits are not overly complex. These advantages sparked

the interest in qudit basic control and led to several proposals and demonstrations in photonic systems [14, 15], superconducting circuits [16, 17], spin systems [18, 19], Trapped ions [20] and Rydberg atoms [21, 22].

In this work, we examine the potential for reducing overhead in quantum error correction codes by utilizing qudits. The essential theoretical background on higher-dimensional quantum computing and the stabilizer formalism is briefly summarized in Section 2. In Section 3, we introduce the smallest stabilizer code capable of correcting any single qudit error [23] and derive a general quantum circuit for it, functional for qudits of all prime dimensions. In Section 4, we present two widely recognized decoders for quantum error correction and modify them for applicability to higher-dimensional error correction codes. Finally, in Section 5, we describe the conducted simulations and analyze the resulting data.

2. MULTILEVEL FAULT TOLERANT QUANTUM COMPUTING: THEORY

2.1. Higher dimensional quantum computing

For a q -dimensional qudit, basis states are indexed by an alphabet of size q , with the general state represented as $|\psi\rangle = \sum_{i=0}^{q-1} \alpha_i |i\rangle$, where $\alpha_i \in \mathbb{C}$ and $\sum_{i=0}^{q-1} |\alpha_i|^2 = 1$. A universal quantum gate set of dimension q is defined as a collection of matrices $U_k \in U(q^n)$ whereby the collective multiplication of its elements enables the approximation of any arbitrary unitary transformation U within the Hilbert space $\mathcal{H}_q^{\otimes n}$ [9]. Numerous propositions of universal gate sets have been proposed [24–26], yet the most pragmatic option to use within the stabilizer formalism is a set containing the Clifford group and the Heisenberg-Weyl gates. The definitions of these gates in general di-

* james.keppens@imec.be

mension q are given by the following expressions:

$$X_q := |n+1\rangle \langle n| \quad , \quad (1)$$

$$Z_q := \omega^n |n\rangle \langle n| \quad , \quad (2)$$

$$F_q := \frac{\omega^{nm}}{\sqrt{q}} |m\rangle \langle n| \quad , \quad (3)$$

$$SUM := |n\rangle |m+n\rangle \langle n| \langle m| \quad , \quad (4)$$

with all numbers taken modulo q and $\omega = e^{\frac{2\pi i}{q}}$ the q 'th root of unity. An additional useful qudit gate is the multiplication gate:

$$M_q := |n(q-1)\rangle \langle n| \quad , \quad (5)$$

it multiplies the initial state with $q-1$ modulo q .

2.2. Stabilizer formalism in higher dimensions

A stabilizer code in q dimensions is characterized by an Abelian subgroup \mathcal{S} of $\mathcal{P}_q^{\otimes n}$ with $-I$ excluded [27, 28]. The codespace is spanned by the eigenspace of \mathcal{S} and detectable errors originating from a particular error basis lead to an exit from the codespace. For the codes regarded in this paper, the correctable error sets are composed by the single qudit Pauli group \mathcal{P}_q :

$$\mathcal{E}_q = \{\omega^a X_q^r Z_q^s\} \text{ with } 0 \leq a, r, s < d \quad (6)$$

and ω^a a phase factor accounting for the different commutations that satisfy the relation:

$$(X_q^r Z_q^s)(X_q^t Z_q^u) = \omega^{st-ru} (X_q^t Z_q^u)(X_q^r Z_q^s) \quad . \quad (7)$$

These errors possess orthogonal eigenspaces with eigenvalues ω^r and can therefore be interpreted as measurable and distinguishable physical observables. An $[[n, k, d]]_q$ stabilizer code of distance d then has n physical qudits representing k logical qudits, generated by $n-k$ generators, a feature only true for prime dimension q [28].

3. PERFECT QUDIT CODES

The smallest error correction code that can correct any single qudit error contains 5 data qudits. This number is determined by the quantum Hamming bound (qHb) and quantum Singleton bound (qSb)[27, 29].

The qHb is a condition generated by simply counting the amount of orthogonal subspaces required to accommodate all errors. In qudit codes with prime dimension, there are q logical states that each need their own q^2-1 subspaces for all possible single error combinations of X_q and Z_q , and one additional subspace for the unperturbed state.

This creates a generalized quantum Hamming bound that prime dimension qudit codes need to satisfy:

$$q((q^2-1)n+1) \leq q^n \quad . \quad (8)$$

The qSb for an $[[n, k, d]]_q$ code is established by the fact that $n-(d-1)$ qudits must contain enough information to be able to reconstruct the q^k logical states and the missing $d-1$ qudits:

$$2(d-1)+k \leq n \quad . \quad (9)$$

The smallest number that meets both conditions is $n=5$, which makes error correction codes with 5 data qudits the so called "perfect" codes. This section describes the construction of the complete quantum circuit for these codes.

3.1. The encoding circuit

The stabilizer generators of these 5-qudit codes are cyclic permutations of $IX_q Z_q Z_q^\dagger X_q^\dagger$. The encoding circuitry can be created by transforming the parity check matrix of the code into one that represents the stabilizer of $|00000\rangle$ [30]. Starting from the general parity check matrix,

$$\left(\begin{array}{ccccc|ccccc} 0 & 0 & q-1 & 0 & 1 & 1 & q-1 & 0 & 0 & 0 \\ 1 & 0 & 0 & q-1 & 0 & 0 & 1 & q-1 & 0 & 0 \\ 0 & 1 & 0 & 0 & q-1 & 0 & 0 & 1 & q-1 & 0 \\ q-1 & 0 & 1 & 0 & 0 & 0 & 0 & 0 & 1 & q-1 \end{array} \right)$$

and applying the following sequence of gates

$$T_1 = I \otimes M_q \otimes F_q \otimes I \otimes M_q F_q \quad ,$$

$$T_2 = SUM^{(0,1)} SUM^{(0,2)} SUM^{(0,4)} \quad ,$$

$$T_3 = I \otimes M_q \otimes F_q \otimes F_q \otimes I \quad ,$$

$$T_4 = SUM^{(1,2)} SUM^{(1,3)} \quad ,$$

$$T_5 = I \otimes I \otimes M_q \otimes F_q \otimes M_q \quad ,$$

$$T_6 = SUM^{(2,3)} SUM^{(2,4)} \quad ,$$

$$T_7 = I \otimes I \otimes I \otimes M_q \otimes F_q \quad ,$$

$$T_8 = SUM^{(3,4)} \quad ,$$

$$T_9 = F_q \otimes F_q \otimes F_q \otimes F_q \otimes I \quad ,$$

results in the check matrix:

$$\left(\begin{array}{ccccc|ccccc} 0 & 0 & 0 & 0 & 0 & 1 & 0 & 0 & 0 & 0 \\ 0 & 0 & 0 & 0 & 0 & 0 & 1 & 0 & 0 & 0 \\ 0 & 0 & 0 & 0 & 0 & 0 & 0 & 1 & 0 & 0 \\ 0 & 0 & 0 & 0 & 0 & 0 & 0 & 0 & 1 & 0 \end{array} \right) .$$

Inverting the sequence of gates and using their conjugate transpose versions, results in a general encoding circuit for perfect qudit codes. The quantum circuitry can be seen on figure 1.

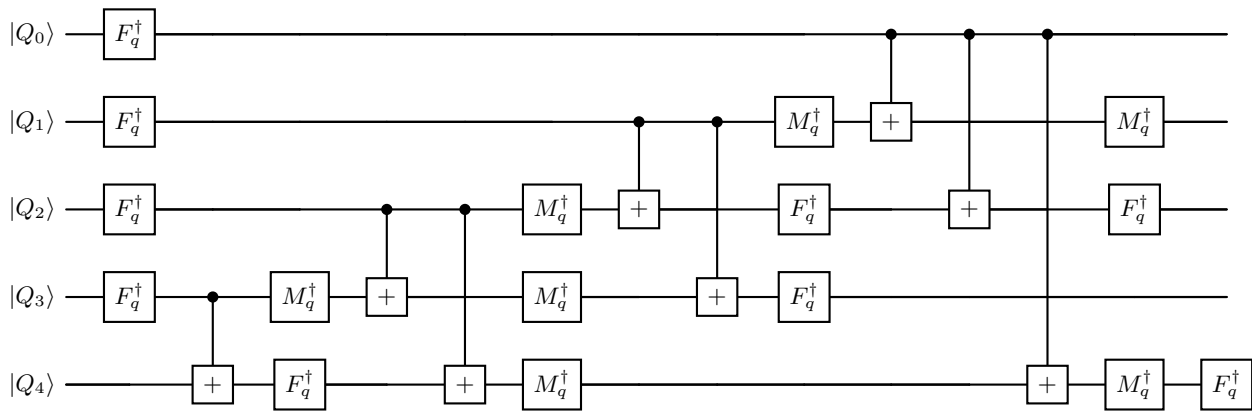


FIG. 1. Encoding circuit of the 5 qudit code, valid for all prime dimensions q .

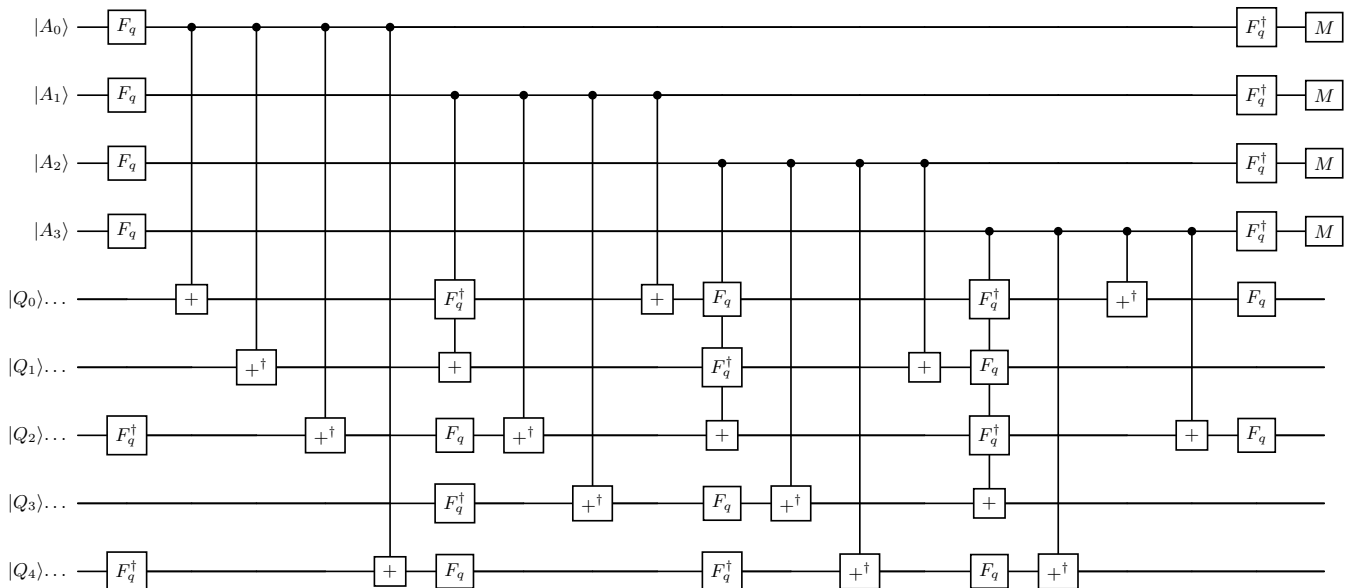


FIG. 2. Quantum circuit representing a single cycle of error syndromes of the 5 qudit code, valid for all prime dimensions q . The circuit is optimized to minimize circuit moments. Q represents a data qudit and A an ancilla qudit. The SUM gates have a dot at the control qudit and a $+$ sign at the target qudit.

3.2. Syndrome measurements

The next part of the quantum circuit should contain the parity checks of the stabilizers. 4 ancilla qudits are added to the circuitry to enable error syndromes that measure the eigenvalues of the stabilizer operators with projection operators. In this way, errors are discretized after each syndrome measurement. The quantum circuit for a single cycle of such an error syndrome can be seen on figure 2. The circuit is optimized to fit as many qudit gates as possible into each time step, minimizing idle moments. It is important to note that for a code utilizing N ancilla units, there are q^N possible syndromes, which makes the use of a simple lookup table impractical and creates the necessity of using more efficient decoding procedures in the form of decoding algorithms.

4. DECODERS AND ADAPTATIONS TO HIGHER DIMENSIONS

In a realistic application of an error correction code, measurement errors can pose considerable problems as they can generate illusory errors and obscure genuine defects. Therefore, it is crucial to execute several syndrome measurement cycles before processing the data using a classical decoding algorithm. The decoder determines a single logical correction tensor to apply at the end of the computation, eliminating the necessity for potentially noisy corrections after each cycle. There are multiple types of decoding algorithms, each with their own decoding fidelities and speeds. Two of them are described and adapted to qudits in this section.

4.1. Minimum-weight perfect matching

The most commonly used and one of the fastest decoders for qubit error correction codes is the minimum-weight perfect matching (MWPM) algorithm [31, 32]. In this algorithm, a detector graph is constructed from the parity check matrix, the nodes represent the ancilla qudits, and the edges represent the possible bit and phase errors. A fast way to find the minimum weight paths between detection events directly in the detector graph, is by using the sparse blossom algorithm, which has an expected running time that is linear in the amount of nodes in the graph [31]¹.

An adaptation to a version that can decode qudit codes can be achieved by creating the detector graph with $q - 1$ nodes for every ancilla, representing all $q - 1$ possible measurable eigenvalues and resulting in a total of $4(q - 1)$ nodes for the 5-qudit code. This method establishes a well-defined correspondence between a higher-dimensional parity check matrix and the associated detector graph, making it generally applicable to all qudit stabilizer error correction codes. An example of matching graphs for dimensions 2, 3 and 5 can be seen on Figures 3, 4 and 5, respectively. However, the

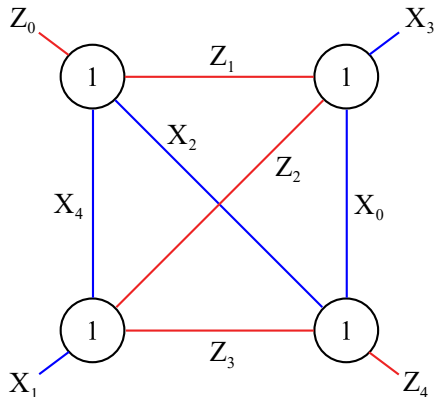


FIG. 3. Matching graph of a single cycle 5 qubit code. All X and Z gates are $q = 2$ -dimensional and act on the i 'th qudit with i being the sub-scripted number. The 4 nodes represent the ancilla qudits that are used to measure the eigenvalue of the stabilizer, which is defined by the single-qubit gates on the edges adjacent to each respective node. Detection events identify specific nodes, which the decoder connects to determine the corresponding error.

disadvantage of this decoder is that it loses efficiency when hyperedge errors such as Y_q are present in the noise model. These errors connect more than 2 nodes in the detector graph and should instead be represented on a hypergraph. Whenever a hyperedge can be decomposed into multiple equally weighted paths, the decoder's likelihood of identifying the right correction decreases. Each

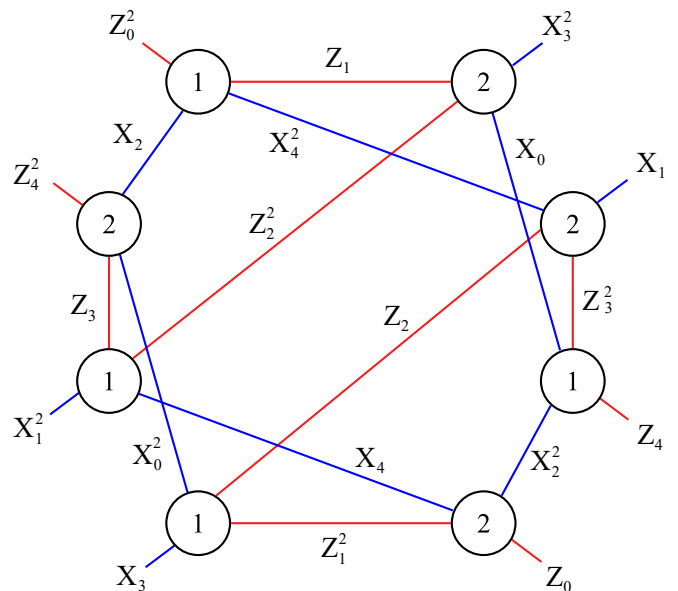


FIG. 4. Matching graph of a single cycle 5 qutrit code. All X and Z gates are $q = 3$ -dimensional and act on the i 'th qudit with i being the sub-scripted number. 8 nodes are now introduced, each representing one of the two measurable eigenvalues of the stabilizers. The edges surrounding each node correspond to the error that gives rise to the eigenvalue in question. The implications on the decoder of this extended matching graph are discussed in the Results section (5.3).

hyperedge error involves either three or four nodes in the matching graph. With a uniform weighting of edges, imposed for example by the depolarizing noise channel, the optimal solution consistently uses the minimum number of edges required to connect these nodes, which is two. In the qubit matching graph, depicted in Figure 3, there exist three distinct configurations for connecting the nodes associated with a hyperedge error using two edges. An example of this is the $Y_0 = X_0 Z_0$ error in figure 3. The three nodes connected by the edges of this error can alternatively be linked by two additional sets of two edges, namely $\{Z_1, Z_4\}$ or $\{X_2, X_3\}$. Conversely, in the qutrit ($q = 3$) matching graph (figure 4) there are only two possible configurations for connecting the nodes associated with a hyperedge error using two edges. This reduction in degeneracy results in a higher error correction fidelity for the MWPM decoder. At even higher dimensions ($q \geq 5$), a clear pattern emerges. The matching graphs become disconnected, with each component resembling the structure observed in qutrit matching graphs, where two complementary eigenvalues are represented per component. Hyperedge errors that span edges in multiple components are efficiently corrected. However, those confined to a single component still suffer from the degeneracy problem.

¹ V2 <https://pymatching.readthedocs.io/en/stable/>

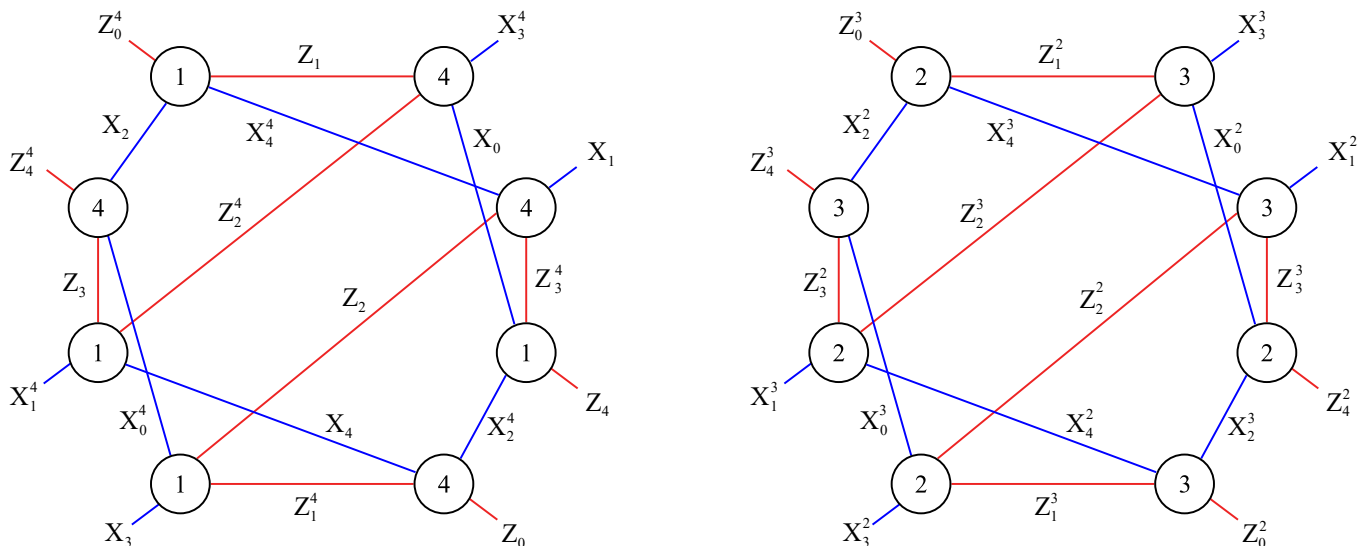


FIG. 5. Matching graph of a single cycle 5 qudit ($q = 5$) code. All X and Z gates are $d = 5$ -dimensional and act on the i 'th qudit with i being the sub-scripted number. This graph contains $4(q - 1) = 16$ nodes, each corresponding to one of the four distinct eigenvalues measurable by the four stabilizers. Furthermore, the graph is disconnected and consists of 2 components with complementary errors and eigenvalues. The implications on the decoder of this extended disconnected matching graph are discussed in the Results section (5.3).

4.2. Belief matching

An effective approach to address hyperedge errors during decoding is through the use of the belief propagation (BP) algorithm [33, 34]. This algorithm uses the parity check matrix H and an initial error probability distribution $P(\mathbf{e})$ to create a Tanner graph and iteratively updates $P(\mathbf{e})$ by passing messages along the edges. The decoder also takes a syndrome \mathbf{s} as input and stops whenever the syndrome equation $H \cdot \mathbf{e} = \mathbf{s}$ is satisfied. This method ensures that hyperedge errors are consistently identified with a specified probability, rather than with a reduced probability as in the MWPM decoder. However, the algorithm ignores measurement errors and does not guarantee a convergence when the graph contains cycles and multiple equally weighted solutions. For that reason, researchers have combined the BP algorithm with secondary codes to ensure a correction whenever BP does not converge. In this work we chose to use the Belief Matching (BM) algorithm that combines belief propagation together with the MWPM algorithm [35].

Adapting the decoder for higher-dimensional qudits is again a matter of adapting the input graph for the decoding algorithm to run on. We can use the same technique of adding virtual detector nodes for the different possible eigenvalues of the stabilizers. In contrast to the MWPM decoder, belief propagation requires a prior error probability distribution, which can become challenging to generate for higher-dimensional systems, as the number of possible error configurations scales with q^2 .

5. SIMULATIONS

To analyze how the qudit codes perform, their circuits were simulated with 3 error syndrome cycles and two different noise models in the quantum circuit simulator Cirq [36]. Although Cirq is designed for qubits, it is extendable to simulate quantum circuits involving qudits by creating custom higher-dimensional gates. We therefore added several Python classes with unitary matrices representing the gates mentioned in section 2.1. During the simulation, the extracted syndromes are input into the aforementioned decoders to gain a correction tensor C , which is applied to the state vector to create a residual error $\Gamma = CE$, with E the actual error. The decoding is considered successful if the final state vector, $\Gamma |\psi\rangle_L$, matches the initial state vector up to the application of a stabilizer.

5.1. Noise models

In the quantum circuit, noise is modeled using the operator-sum approach by introducing time slices with Kraus operators that evolve the density matrix via $\rho \rightarrow \sum_i K_i \rho K_i^\dagger$. In this representation, the single qudit depolarization noise channel with Pauli operators is described by the mapping [37]:

$$\rho \rightarrow \left(1 - p \frac{(q^2 - 1)}{q^2}\right) \rho + \frac{p}{q^2} \sum_{i=1}^{q^2-1} P_i \rho P_i^\dagger, \quad (10)$$

with P_i one of the $q^2 - 1$ possible Pauli errors and p the probability of having a depolarizing error. Note that the overall robustness of the qudit depends on the dimension as the chance of no error is $1 - p(q^2 - 1)/q^2$. Similarly, the two-qudit depolarizing channel is represented by the map:

$$\rho \longrightarrow \left(1 - p_2 \frac{(q^4 - 1)}{q^4}\right) \rho + \frac{p_2}{q^4} \left(\sum_{i=1}^{q^2-1} \sum_{j=1}^{q^2-1} P_j P_i \rho P_i^\dagger P_j^\dagger + \sum_{i=1}^{q^2-1} P_i \rho P_i^\dagger + \sum_{j=1}^{q^2-1} P_j \rho P_j^\dagger \right), \quad (11)$$

with P_i and P_j one of the $q^2 - 1$ possible Pauli errors acting on two different qudits and p_2 the chance on a two-qudit depolarization error. Lastly, the measurement error channel is given by:

$$\rho \longrightarrow (1 - p_m) \rho + p_m X_q \rho X_q^\dagger. \quad (12)$$

These noise channels are used to create two noise models. The first is the standard depolarization noise model often used for benchmarking error-correcting codes and decoders. In this model, single-qudit depolarization noise is applied to all data qudits prior to each cycle's syndrome extraction, while assuming ideal measurements with no errors. In this noise model, the input parameter p corresponds to the physical error rate of a single physical qudit.

The second noise model is designed to better reflect the behavior of physical quantum circuits by incorporating errors at each timestep of the circuit. During idle periods and single-qudit gate operations, qudits experience single-qudit depolarizing noise. Conversely, when a qudit participates in a two-qudit gate operation, it is subject to two-qudit depolarizing noise. Ancilla qudits are modeled to undergo bit-flip errors prior to their readout. All error probabilities are uniformly set to a value p , as detailed information regarding qudit lifetimes, dephasing times, single-qudit gate and two-qudit gate fidelities for a single physical system is currently unavailable. The primary purpose of these simulations is to compare the performance of error correction codes across different qudit dimensions and decoding algorithms. As more precise data on qudit parameters become available, the model can be refined to enable more sophisticated and accurate simulations.

5.2. Error ratio

To facilitate the comparison of logical error rates across quantum error correction codes of different dimensions, we introduce a scaled error ratio. This metric accounts for the fact that certain quantum algorithms, such as the Quantum Fourier Transform (QFT) [38], require $\log_2(q)$ fewer logical qudits of dimension q than logical qubits.

The QFT algorithm is foundational for many quantum algorithms, making it a relevant benchmark. Consider a QFT algorithm that requires N logical qubits, each with a logical error rate P_{L2} . The expected number of logical errors during the algorithm's execution is $N \cdot P_{L2}$, a quantity that must remain significantly below one to ensure computational reliability. When using logical qudits of dimension q , the same algorithm would only require $N/\log_2(q)$ logical qudits. Thus, the corresponding average number of errors is $\frac{N \cdot P_{Ld}}{\log_2(q)}$, where P_{Ld} denotes the logical error rate for qudits. To compare the error performance across dimensions without dependence on N , we define the scaled error ratio as:

$$R = \frac{P_{Lq}}{P_{L2} \cdot \log_2(q)}. \quad (13)$$

This ratio normalizes the error rates by accounting for the dimensional advantage of qudits in reducing the number of required logical units. A ratio R lower than one indicates that the expected number of average logical errors during the computation is smaller for qudits of dimension q than for qubits. It should be noted that the error correction codes simulated in this study are restricted to a code distance of 3. Although this distance can, in principle, be increased to reduce the logical error rate when the physical error rate is below a certain threshold, such simulations are currently computationally infeasible. The exponential increase in computational complexity with higher qudit dimension prevents us from exploring this phenomenon, limiting us to a comparison of error rates for codes with a fixed distance of 3.

5.3. Results

The simulation results are detailed in this section. Two noise models were explored. The logical error rates of error correction codes across different dimensions are subsequently compared, and the observed differences are examined in relation to the nature of the errors and the decoders utilized.

5.3.1. Standard depolarization noise

The results of the simulations with standard depolarization noise can be seen in Figure 6. The data points for dimensions 2, 3, and 5 are based on averages computed from 400,000 simulated samples, ensuring a reliable convergence of the results. The error bars, representing 90% confidence intervals, are smaller than the marker sizes for these dimensions. In contrast, the data point for $q = 7$ is derived from only 5,000 samples and is included solely to confirm observed trends.

An error correction code is considered effective when its

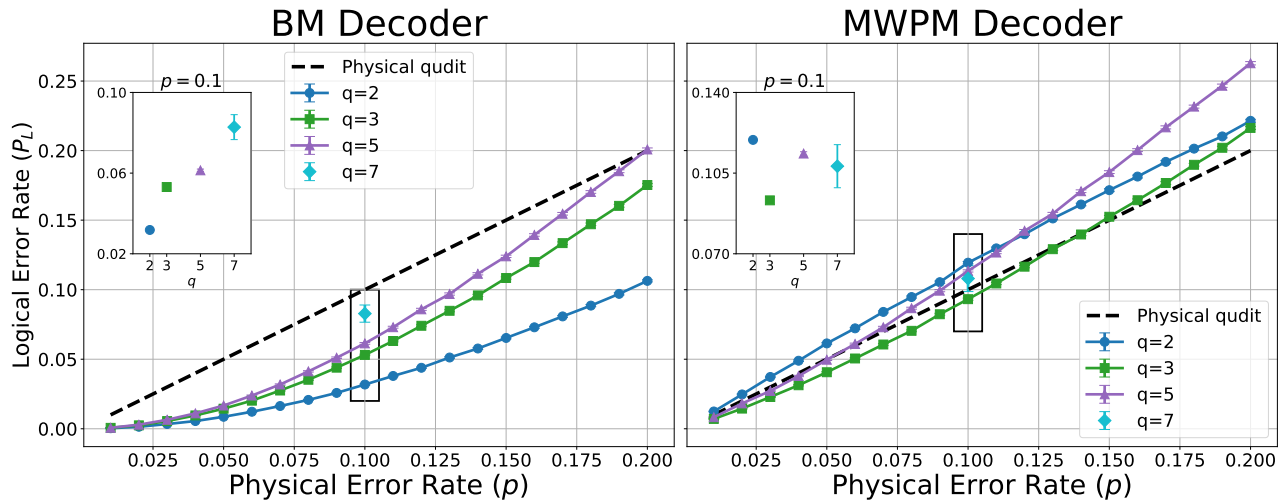


FIG. 6. Logical error rates obtained in simulations with standard depolarization noise of the 3-cycle 5-qudit code using qudits of dimensions 2, 3, 5, and 7 decoded with the MWPM and BM decoders. The black dashed line represents the error rate of a single physical qudit. The error bars correspond to the 90% confidence intervals.

logical error rate (P_L) is lower than that of an individual physical qudit, which asymptotically approaches p in higher-dimensional systems for this noise channel. In Figure 6 it can be seen that despite having a distance of only three, the five-qudit code achieves lower logical error rates compared to a single physical qudit when decoded by the BM decoder.

The fact that the BM decoder achieves lower P_L 's than the MWPM decoder can be attributed to its more efficient correction of hyperedge Y-errors. The BM decoder is, in fact, capable of correcting every individual qudit error, making the dependence of the error channel on the qudit dimension the sole factor influencing the logical error rate. Consequently, the logical error rates of the BM decoder are higher for higher dimensions. These results offer clear confirmation that the adapted BM decoder functions correctly for higher-dimensional qudit error correction codes.

Interestingly, the less effective, but faster, MWPM decoder initially shows lower logical error rates for the higher dimensional codes than the qubit version. This feature arises from the fact that hyperedge errors in higher dimensions can be decomposed into fewer, equally weighted paths, as was described in section 4.1. We additionally observe that for ququints ($q = 5$), a larger fraction of Y-type errors remains uncorrected compared to the qutrit case and at higher error probabilities the influence of dimensionality in the noise channel becomes the dominant factor.

An additional data point for qudits of dimension $q = 7$ at a physical error rate of $p = 0.1$ is shown on the insets of Figure 6. This data point is based on a limited number of simulations and is used to provide some confirmation of expected trends. More specifically, the BM-decoded data point shows a slightly higher logical error rate, which aligns with the expectation that error like-

lihood increases with dimensionality. For the MWPM-decoded data point, the logical error rate falls between those of qubits and qutrits. This behavior can be attributed to the structure of the matching graph, which is similar to that of the ququint case, consisting of a disconnected graph with three components. A more comprehensive analysis of qudit codes with dimensions $q = 7$ and higher would necessitate increased computational resources or further optimization of the simulation process.

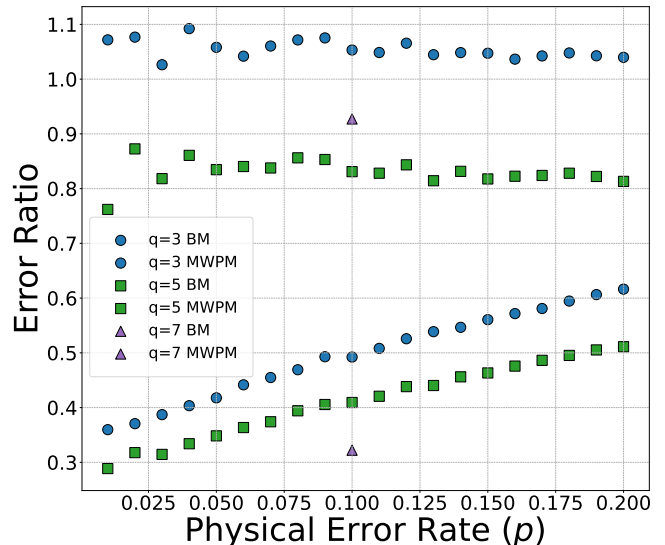


FIG. 7. Error ratios R calculated with the means of the simulated logical error rates of the 5-qudit error correction codes with standard depolarization noise decoded by the BM and MWPM decoder.

Figure 7 presents the newly introduced error ratios. This

ratio quantifies the comparison between the average errors of logical qudit ensembles used to perform a specific computation and the average errors incurred when the same computation is carried out with logical qubits that are error corrected with the same adapted decoder. Error ratios for dimension-3 qudits are depicted in blue, those for dimension-5 qudits are shown in green, and the illustrational error ratio for dimension-7 qudits can be seen in purple.

The error ratio R is highest for qutrits, exceeding a value of one, which indicates a disadvantage with respect to qubits. However, when the dimension increases to 5, further reducing the number of logical units needed for the same computation, the error ratio drops below one, averaging at 0.831. The larger state spaces of these higher-dimensional logical qudits offer enough of an advantage to overcome the dimensionality dependence of the error channel. This indicates that it makes perfect sense to increase qudit dimension when using low distance codes with a successfully adapted error correction code. Exploring this advantage at higher code distances and providing a detailed overhead analysis with threshold physical error rates is left for future work, once the challenges related to computational complexity have been addressed.

The adapted MWPM decoder was able to capture more errors in higher dimensions, resulting in logical error rates that were already comparable to, or better than, the logical error rates observed for qubits. This added advantage, combined with the reduced number of logical units needed to perform computations, leads to even more favorable error ratios, further encouraging the adoption of higher-dimensional error correction codes.

5.3.2. Circuit-level noise

Figure 8 illustrates the simulated logical error rates for the 3-cycle 5-qudit error correction codes with circuit-level noise decoded with the MWPM and BM decoders, as well as the logical error rate without error correction. Both decoders exhibit comparable performance, noticeably improving upon the scenario without applying the correction tensor. The variations in error rates are largely influenced by the dimensionality dependence of the error channel. Additionally, we observe that the MWPM decoder's ability to correct a greater number of hyperedge Y -type errors is overshadowed by the fact that the code cannot correct two or more errors in a single cycle, which for example happens for any two-qudit error.

Figure 9 showcases the error ratios calculated with the logical error rates from the circuit-level noise simulations. All configurations exhibit relatively constant error ratios across the range of physical error rates (p). The average error ratios, in descending order, are as follows: 0.873 for the BM decoder with qutrits, 0.743 for the

MWPM decoder with qutrits, 0.650 for the BM decoder with ququints, and 0.568 for the MWPM decoder with ququints. Notably, all values are below one, signifying an advantage over qubit-based codes for the simulated code distance of 3.

6. CONCLUSION AND OUTLOOK

In this work, we have created a general encoding circuit for the 5-qudit error correction code and performed simulations of syndrome measurements with two different noise models. The extracted syndromes have been error corrected with adapted versions of the MWPM and BM decoder that work for any prime qudit dimension. Our analysis reveals that under the standard depolarization noise model, the adapted BM decoder consistently corrects all types of single qudit errors and makes the 5-qudit code with a distance of 3 outperform a single physical qudit for all dimensions. The adapted MWPM decoder demonstrates lower performance compared to the BM decoder, primarily due to its reduced effectiveness in correcting hyperedge errors. Interestingly, this disadvantage becomes less pronounced at higher dimensions, as the larger matching graphs exhibit fewer degenerate solutions. Under circuit-level noise, both decoders demonstrated similar performance, largely due to the increased likelihood of uncorrectable two-qudit errors in the distance-3 codes. Furthermore, we introduced the error ratio R to facilitate a meaningful comparison of logical error rates. This metric accounts for the fact that fewer higher-dimensional logical qudits are needed to perform the same computational tasks as qubits. Most of the calculated ratios were below one, indicating fewer average errors when computations are performed using higher-dimensional logical qudits.

To facilitate simulations of qudit error correction codes with greater distances and to identify error rate thresholds, it is necessary to address the computational complexity of the problem. This could be achieved, for instance, by extending stabilizer simulation frameworks, such as STIM [39], to work for qudits, an endeavor left for future work. Additionally, we propose the adaptation of other decoders, such as the maximum likelihood decoder, to higher-dimensional systems.

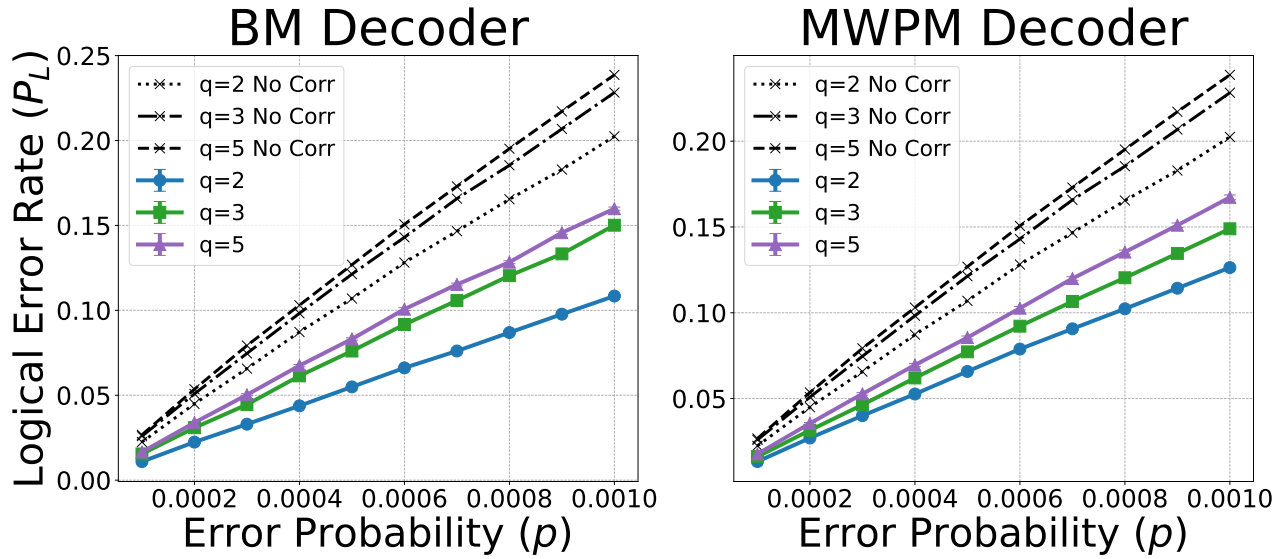


FIG. 8. Logical error rates obtained in simulations with circuit-level noise of the 5-qudit code using qudits of dimensions 2, 3, and 5, decoded with the MWPM and BM decoders. The black dashed lines represent the logical error rates without any error correction. The error bars correspond to the 90% confidence intervals and are smaller than the marker sizes.

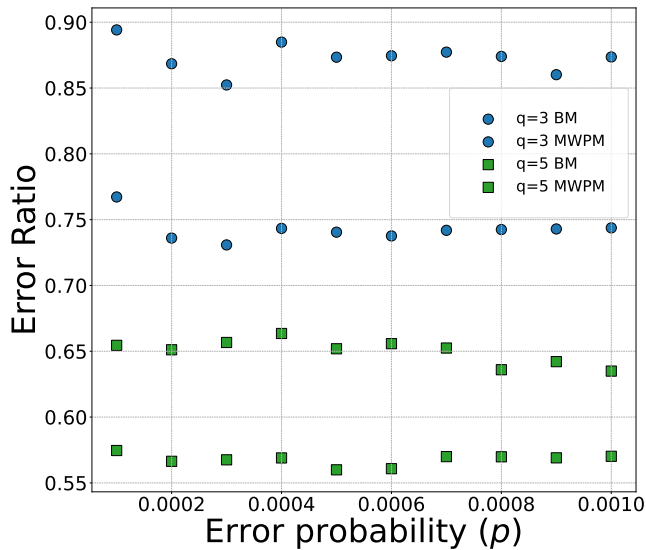


FIG. 9. Error ratios R calculated with the means of the simulated logical error rates of the 5-qudit error correction codes with circuit-level noise decoded by the BM and MWPM decoder.

[1] W. H. Zurek, *Physics Today* **44**, 3644 (1991).
 [2] R. Acharya, et al., G. Q. AI, and Collaborators, *Nature* (2024).
 [3] S. B. Bravyi, A. Y. Kitaev, and L. D. Landau, (1998), arXiv:quant-ph/9811052.

[4] A. G. Fowler, M. Mariantoni, J. M. Martinis, and A. N. Cleland, *Phys. Rev. A* **86**, 032324 (2012).
 [5] P. Panteleev and G. Kalachev, in *Proceedings of the 54th Annual ACM SIGACT Symposium on Theory of Computing*, STOC 2022 (Association for Computing Machin-

- ery, New York, NY, USA, 2022) p. 375388.
- [6] S. Bravyi, A. W. Cross, J. M. Gambetta, D. Maslov, P. Rall, and T. J. Yoder, *Nature* **627**, 778782 (2024).
- [7] B. Field and T. Simula, *Quantum Science and Technology* **3**, 045004 (2018).
- [8] A. Schotte, G. Zhu, L. Burgelman, and F. Verstraete, *Physical Review X* **12**, 021012 (2022).
- [9] Y. Wang, Z. Hu, B. C. Sanders, and S. Kais, *Frontiers in Physics* **8** (2020).
- [10] M. Huber and J. I. de Vicente, *Physical Review Letters* **110**, 030501 (2013).
- [11] P. Gokhale, J. M. Baker, C. Duckering, N. C. Brown, K. R. Brown, and F. T. Chong, in *Proceedings of the 46th International Symposium on Computer Architecture* (ACM, Phoenix Arizona, 2019) p. 554566.
- [12] E. T. Campbell, H. Anwar, and D. E. Browne, *Physical Review X* **2**, 041021 (2012).
- [13] E. T. Campbell, *Physical Review Letters* **113**, 230501 (2014).
- [14] Y. Chi, J. Huang, Z. Zhang, J. Mao, Z. Zhou, X. Chen, C. Zhai, J. Bao, T. Dai, H. Yuan, M. Zhang, D. Dai, B. Tang, Y. Yang, Z. Li, Y. Ding, L. K. Oxenlwe, M. G. Thompson, J. L. O'Brien, Y. Li, Q. Gong, and J. Wang, *Nature Communications* **13** (2022).
- [15] B. P. Lanyon, M. Barbieri, M. P. Almeida, T. Jennewein, T. C. Ralph, K. J. Resch, G. J. Pryde, J. L. O'Brien, A. Gilchrist, and A. G. White, *Nature Physics* **5**, 134140 (2009).
- [16] R. Bianchetti, S. Filipp, M. Baur, J. M. Fink, C. Lang, L. Steffen, M. Boissonneault, A. Blais, and A. Wallraff, *Physical Review Letters* **105**, 223601 (2010).
- [17] M. Kononenko, M. A. Yurtalan, S. Ren, J. Shi, S. Ashhab, and A. Lupascu, *Physical Review Research* **3**, L042007 (2021).
- [18] I. Fernández de Fuentes, T. Botzem, M. A. I. Johnson, A. Vaartjes, S. Asaad, V. Mourik, F. E. Hudson, K. M. Itoh, B. C. Johnson, A. M. Jakob, J. C. McCallum, D. N. Jamieson, A. S. Dzurak, and A. Morello, *Nature Communications* **15**, 1380 (2024).
- [19] C. Godfrin, A. Ferhat, R. Ballou, S. Klyatskaya, M. Ruben, W. Wernsdorfer, and F. Balestro, *Physical Review Letters* **119**, 187702 (2017).
- [20] M. Ringbauer, M. Meth, L. Postler, R. Stricker, R. Blatt, P. Schindler, and T. Monz, *Nature Physics* **18**, 10531057 (2022).
- [21] J. R. Weggemans, A. Urech, A. Rausch, R. Spreew, R. Boucherie, F. Schreck, K. Schoutens, J. Min, and F. Speelman, *Quantum* **6**, 687 (2022).
- [22] J. Ahn, T. C. Weinacht, and P. H. Bucksbaum, *Science* **287**, 463465 (2000).
- [23] R. Laflamme, C. Miquel, J. P. Paz, and W. H. Zurek, *Phys. Rev. Lett.* **77**, 198 (1996).
- [24] A. Muthukrishnan and C. R. Stroud, *Physical Review A* **62**, 052309 (2000).
- [25] G. Brennen, D. O'Leary, and S. Bullock, *Physical Review A* **71**, 052318 (2005).
- [26] M. Luo and X. Wang, *Science China: Physics, Mechanics and Astronomy* **57**, 17121717 (2014).
- [27] D. Gottesman, *Stabilizer Codes and Quantum Error Correction*, Ph.D. thesis, California Institute of Technology (1997), arXiv:quant-ph/9705052.
- [28] D. Gottesman, in *Quantum Computing and Quantum Communications*, edited by C. P. Williams (Springer Berlin Heidelberg, Berlin, Heidelberg, 1999) pp. 302–313.
- [29] E. Knill and R. Laflamme, *Phys. Rev. A* **55**, 900 (1997).
- [30] M. Grassl, M. R. Otteler, and T. Beth, *International Journal of Foundations of Computer Science* (2002).
- [31] O. Higgott, *ACM Transactions on Quantum Computing* **3** (2022).
- [32] A. V. Antipov, E. O. Kiktenko, and A. K. Fedorov, *Phys. Rev. A* **107**, 032403 (2023).
- [33] B. Criger and I. Ashraf, *Quantum* **2**, 102 (2018).
- [34] J. Roffe, D. R. White, S. Burton, and E. Campbell, *Physical Review Research* **2**, 10.1103/physrevresearch.2.043423 (2020).
- [35] O. Higgott, T. C. Bohdanowicz, A. Kubica, S. T. Flammia, and E. T. Campbell, *Physical Review X* **13**, 031007 (2023).
- [36] C. Developers, *Cirq* (2024).
- [37] M. M. Wilde, *Quantum Information Theory*, 1st ed. (Cambridge University Press, 2013).
- [38] Z. Zilic and K. Radecka, *IEEE Transactions on Computers* **56**, 202207 (2007).
- [39] C. Gidney, *Quantum* **5**, 497 (2021).